International Journal of Advanced Information Science and Technology (IJAIST) ISSN: 2319:2682
Vol.6, No.7, July 2017 DOI:10.15693/ijaist/2017.v6i11.77-94

Exploration of Laser Jet Welding by Using CFD

K. Anusha[1], A. Santhosh[2]

[1, 2,] Assistant Professor,
[1, 2] Department of Mechanical Engineering,
[1]Samskruti College of Engineering &Technology,
[2]Geethanjali College of Engineering &Technology,
[1, 2,] Hyderabad, India.
Email: anusha.kuntala@yahoo.com, aadharisanthosh@gmail.com

Abstract: Since low aspect ratio welds can be made with Conduction mode welding, it is used in thin sheet welding. The weld geometry and microstructure depend on the temperature distribution and the cooling rates. Experimental determination of temperatures in the work-piece through the use of thermocouples, can provide data for a limited number of points and is time consuming and expensive. Numerical modeling of heat transfer and fluid flow in laser beam welding can provide previously unavailable information about the temperature distribution and thermal cycles at all points in the computational domain in a relatively short time and at low cost. A critical review of the available literature indicates the following problems with the numerical models of conduction mode welding. (1) There is no comprehensive three-dimensional model of conduction mode laser beam welding (LBW) available in literature (coded). (2) While models of conduction mode laser beam welding (LBW) have been proposed, very few has been tested for the welding of various materials with thin plates. The goal of this dissertation is to address these important issues. In this dissertation, a comprehensive two-dimensional heat transfer model based on energy conservation equations is solved to study the shape of weld pool. Weld thermal cycle and weld pool geometry considering fluid flow for laser spot welding of mild steel for two dimensional, turbulent and transient models based on mass, momentum and energy equations is modeled to study temperature and velocity fields along with weld pool. A moving Gaussian heat source is considered as laser beam. To make model computationally efficient half of the geometry is modeled. In case of welding with fluid flow surface tension and gravity forces are considered for the calculation of transient weld pool convection. A finite volume scheme with fixed time stepping is used for the calculations. The observed weld pool dimension is compared for different beam power and beam radius applied as heat source. The behavior of the mushy zone, i.e., the solid-liquid two phase region, during heating and cooling is studied. Results show information about the weld pool shape, maximum temperature and velocity vectors. This data is useful for determining the solidification morphology and the scale of the solidification sub structure.

Key words: laser beam welding, weld pool shape, maximum temperature, velocity vectors, etc.

I.INTRODUCTION

Laser welding has become a significant industrial process because there are many outstanding advantages in using laser welding over other widely used bonding technologies. As an alternative to the common adhesives or solders used for the joining process, laser welding offers a number of attractive features such as high weld strength to weld size ratio, reliability, and minimal heat-affected zone. These provide the benefits of low heat distortion, a noncontact process, repeatability, ability to automate, and high throughput. For these reasons, the applications of laser beam welding have broadened in the past decades. Here laser welding is carried out on small thickness where the thickness of plates is in microns which need a small heat affected zone. Lasers are well suited for welding with small length scale because they can deliver a controlled amount of energy to very small components with a high degree of precision. Laser welding is generally carried out in two modes; conduction mode welding and keyhole mode welding. In keyhole mode of welding the material is heat above its vaporization temperature forming plasma leading to deeper weld pools and hence are used with thick plates. In conduction mode welding, the material is heated below its vaporization temperature leading to small weld depths. Conduction mode is mostly preferred in micro-welds due so as to keep weld free of contamination and blow holes caused during solidification of the material.

Laser welds behave very differently from other welding process due to its small heat affected zone and the interaction with material is in milliseconds. Such short time makes it much more difficult to make physical measurements of the above-mentioned important parameters. Thus, to investigate these parameters at micro level of length and time scale numerical methods are required where the domain is divided into fine grids and considering very small-time steps makes it possible to study the behavior of these parameters at small time scales.

1.1 Statement of Problem: A critical review of the available literature indicates the following problems with the numerical models of conduction mode welding.
(1) There is no comprehensive three-dimensional model of conduction mode laser beam welding (LBW) available in literature (coded). (2) While models of conduction mode laser beam welding (LBW) have been proposed, very few has been tested for the welding of various materials with thin plates.

1.2 Objective of the present Work: The main objective is to simulate the 2D model of laser jet welding is in ANSYS FLUENT. The heat source as laser beam is applied by defining a UDF and hooking it to the top boundary. To model phase change in FLUENT solidification and melting model with mushy zone constant of value 10^5 is used. For numerical modeling of the phase change process enthalpy method is used where the enthalpy at grid points is calculated and from these enthalpy values temperatures at corresponding points are calculated. To track solid liquid interface volume of fluid method is used where volume fraction of the cells is calculated from corresponding enthalpy values.

II.HEAT TRANSFER IN LASER WELDING

The coherent laser beam at a particular wave length is focused on the work piece to be welded. This beam has an energy corresponding to product of Planck's constant and frequency of the beam, which is absorbed by the surface of the wok piece depending on the absorptivity of the material. The surface temperature of the work piece which is initially at ambient temperature starts increasing with time till it reaches the melting point of the material. The flow of energy up to this point is mainly due to conduction.

Radial temperature gradients on the order of 10^2–10^4K/mm develop between the center of the forming melt pool and the cooler solid/melt interface. In most materials, the coefficient of surface tension increases with a decrease in temperature; surface tension gradients are therefore induced that drive fluid flow from the center of the melt towards the edges called Marangoni flow, whereas certain elements invert the relationship between surface tension and temperature leading to a reversal of the fluid flow geometry. Marangoni flow is the dominant convection mechanism in a laser melted pool.

2.1 Modes of laser welding

Depending on the maximum temperature obtained by heating the material by laser beam and its melting and vaporization, laser welding is categorized into two types as a) Conduction mode welding and, b) Keyhole mode welding.

2.1.1 Conduction welding

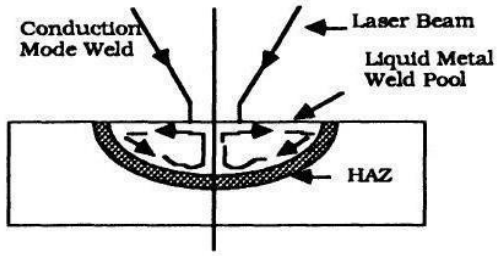

Figure 2.1: Conduction mode welding

This occurs when the power density at a given welding speed is insufficient to cause boiling. The weld pool has strong stirring forces resulting from variation in surface tension with temperature. Most surface treatments in which melting occur employ an out of focus beam, which results in conduction limited weld beads. This mode of welding is used in thin plates as weld depth achieved is very less. The quality of welds forms in this mode is better than keyhole mode and free of contaminants.

2.1.2 Keyhole welding

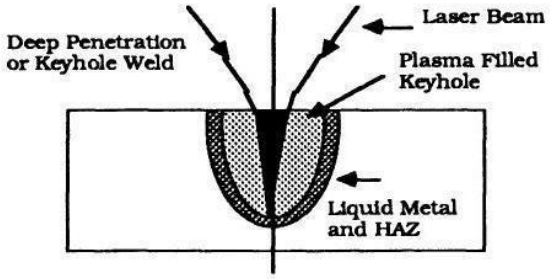

Figure 2.2: Keyhole mode welding

Keyhole mode laser welding of metals requires laser irradiance in excess of 106 W/cm^2. During this

process, the laser beam melts through the metal work piece thickness and produces a narrow cylinder of liquid metal. Furthermore, vaporization of the liquid through a finite thickness occurs, producing a column of metal vapor. The vapor column, commonly referred to as a vapor cavity or keyhole, is surrounded by liquid metal. Because of temperature gradients existing along surface and subsurface liquid layers, the surface tension varies dramatically along these liquid layers, promoting localized convection.

When the work piece is translated past the laser beam, the metal along the leading edge of the keyhole is melted through its entire thickness. The liquid metal flows around and along the base of the keyhole, eventually solidifying at the trailing edge. The stability of the keyhole is based on laser irradiance and welding speed.

2.2 Numerical modeling of solidification and melting

Due to the strong nonlinearity of solid-liquid phase change phenomena and the moving boundary, the problems that can be solved via the analytical method are very limited. Exact solutions and some approximate solutions for melting and solidification have been developed. The limitation of these methods is that they apply to conduction-controlled one-dimensional problems. Generally, the analytical method will not work for two- or three-dimensional problems. This is particularly true for convection-controlled phase change processes. Most real applications of phase change occur in complex two- or three-dimensional geometries.

In addition, natural convection in the liquid phase often plays a significant role in the phase-change processes. For such complex solid-liquid phase-change processes, analytical solutions will not work. Therefore, it is necessary to employ numerical methods. A large number of numerical methods have been developed and they can be divided into two groups.

The first group is called moving boundary problems. For this group, transformed coordinate systems or deformed grids are employed to deal with the location of the solid-liquid interface. In this methodology, complex geometric regions of solid or liquid phases are transformed into fixed, simple geometric regions through the coordinate transformation technique. At the same time, the governing equations and the boundary conditions become more complicated. Such methods also deal successfully with multidimensional one-region or two-region problems with or without natural convection in the liquid phase.

The disadvantage of these methods is that they are often difficult to program and thus require a significant amount of computer time.

The second group is called the fixed-grid solution. In these methods, the governing equations are written for the entire phase change region, including liquid and solid phases. The location of the solid-liquid interface is determined after the converged temperature distribution is obtained. The three principal important methods in this group are,

a) The enthalpy method (Shamsunder and Sparrow, 1975; Crank, 1984),
b) The equivalent heat capacity method (Bonacina et al., 1973), and
c) The temperature-transforming model (Cao and Faghri, 1990).

The temperature transforming model has the advantages of both the enthalpy method and the equivalent heat capacity method and can also account for the effect of natural convection in the liquid phase. The most significant advantage of the weak solution, as compared with the strong numerical solution, is its simplicity. Various fixed-grid numerical solutions of the solid-liquid phase problem are described as below.

2.2.1 Enthalpy method

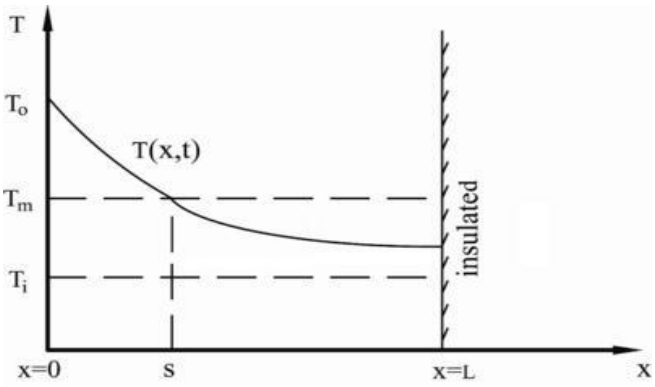

Figure 2.3: Conduction controlled melting in a finite slab

In this methodology, the governing energy equation is written for the entire region of the PCM, including solid and liquid phases and the interface. The enthalpy method is introduced by analyzing a conduction-controlled, two-region melting problem in a finite slab, as shown in Fig.2.3. It is assumed that the densities of the liquid and solid phase are identical ($\rho_s = \rho_l$). The energy equation can be written as

$$h$$

The enthalpy h is a function of temperature

$$h(\quad) = \{ \quad (\quad - \quad) + h \quad , \quad > \quad , \quad < \quad (\quad - \quad),$$

At the melting point of the PCM, the enthalpies of solid and liquid phases at the melting point are 0 and h_{sl} respectively; the is a jump of enthalpy equal to the latent heat of the PCM. The thermal conductivity of the PCM, k can be expressed as

$$(\quad) = \{ \quad , \quad <$$

Solving for temperature T, by substituting k (T) and h (T) from above equations in energy equation yields,

$$+ \quad \frac{h}{\quad} \quad , \qquad h \leq 0$$

$$0 < h < h$$

2.2.2 Equivalent heat capacity method

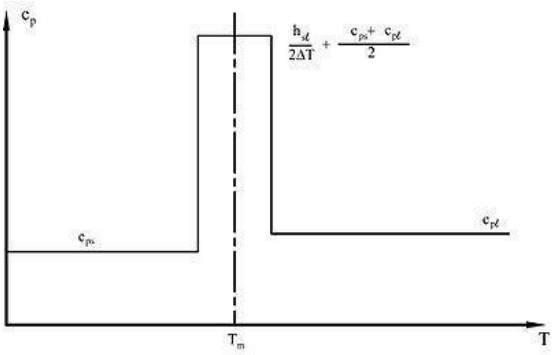

Figure2.4: Specific heat for equivalent heat capacity method

In the equivalent heat capacity method, it is assumed that the melting or solidification processes occur over a temperature range ($T_m - \Delta T$, $T_m + \Delta T$) instead of at a single temperature T_m. For a multicomponent system, ΔT can be chosen based on the range of phase change temperature. For a single-component with well-defined melting point, ΔT should be as small as possible. Also, the latent heat is converted to an equivalent heat capacity of the PCM in the assumed temperature range. Thus, the specific heat of the PCM can be expressed as

$$(\quad)$$

$$= \{ \quad \frac{h}{\quad} \quad + \quad \frac{\quad}{\quad} \quad , \qquad - \Delta < < + \Delta$$

$$< - \Delta \qquad > + \Delta$$

This assumes that temperature of the PCM is changed from (Tm – ΔT) to (Tm + ΔT) when latent heat, h_{sl}, is absorbed by the PCM during melting. During the solidification process, the PCM releases the latent heat and its temperature decreases from Tm + ΔT to Tm − ΔT. The equivalent specific heat in the mushy zone (Tm − ΔT < T < Tm + ΔT) includes the effect of both latent heat (the first term) and sensible heat (the second term). The relationship between specific heat and temperature in the equivalent heat capacity method is plotted in Fig.2.4. For a three-dimensional conduction-controlled melting/solidification problem in the Cartesian coordinate system, the energy equation for the entire region of the PCM can be expressed as

$$= \quad (\quad) + \quad (\quad) + \quad (\quad)$$

Where the thermal conductivity in the equation is a function of temperature T. Assuming that the thermal conductivity of the PCM in the two-phase region is a linear function of temperature, $(\quad)$

$$< \qquad - \Delta$$

$$= \quad \{ + \quad (\quad - + \Delta), - \Delta < < + \Delta \quad 2 \Delta$$

$$> \qquad + \Delta$$

The advantage of the equivalent heat capacity model is its simplicity. The energy equation above is simply the nonlinear heat conduction equation, and it appears that a conventional computational methodology for conduction problems is adequate for solving a solid-liquid phase change problem. However, studies have revealed difficulties in the selection of time step, Δt, grid size, (Δx, Δy, Δz) and the phase change temperature range, ΔT. If these variables cannot be properly selected, the predicted location of the solid-liquid interface and the temperature may include some unrealistic oscillation. Therefore, although the equivalent heat capacity model leads to simple code development, it is not used as widely as the enthalpy model.

2.2.3 Temperature transforming model

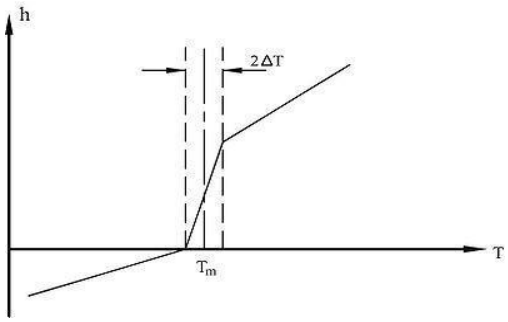

Figure 2.5: Dependence of enthalpy on temperature for phase change occurring over a range of temperature

The temperature-transforming model proposed by Cao and Faghri (1990) combines the advantages of the enthalpy and equivalent heat capacity models. For a three-dimensional conduction-controlled phase change problem, the governing equation in enthalpy form is

$$\frac{\partial h}{\partial} = \frac{\partial}{\partial}\left(\frac{\partial}{\partial}\right) + \frac{\partial}{\partial}\left(\frac{\partial}{\partial}\right) + \frac{\partial}{\partial}\left(\frac{\partial}{\partial}\right)$$

For a phase change occurring over a temperature range (T_m-ΔT, T_m+ΔT) with the specific heats assumed to be constant for each phase, the relationship between enthalpy and temperature can be plotted as in fig.2.5. This relationship can be analytically expressed as

$$h(T) = \begin{cases} (T - T_m) + (\Delta T), & T < T_m - \Delta T \\ \left(\frac{c_{p,s} + c_{p,l}}{2} + \frac{b_s + b_l}{2\Delta T}\right)(T - T_m) + \frac{b_s + b_l}{2}\Delta T + L, & T_m - \Delta T \le T \le T_m + \Delta T \\ (T - T_m) + (\Delta T) + L, & T > T_m + \Delta T \end{cases}$$

By defining specific heat in the mushy zone as

$$c_p = c_{p,s} + \frac{b_s + b_l}{2}$$

Therefore,

$$h(T) = \begin{cases} (T - T_m) + (\Delta T), & T < T_m - \Delta T \\ \left(c_{p,s} + \frac{b_s + b_l}{2\Delta T}\right)(T - T_m) + \Delta T + \frac{b_s + b_l}{2}, & T_m - \Delta T \le T \le T_m + \Delta T \\ (T - T_m) + (\Delta T) + L, & T > T_m + \Delta T \end{cases}$$

This can be written as,

$$h(T) = c_p(T)(T - T_m) + b(T)$$

Where Cp(T) and b(T) can be determined by,

$$b(T) = \begin{cases} (\Delta T), & T < T_m - \Delta T \\ \frac{b_s + b_l}{2}, & T_m - \Delta T \le T \le T_m + \Delta T \\ L, & T > T_m + \Delta T \end{cases}$$

$$c_p(T) = \begin{cases} (\Delta T), & T < T_m - \Delta T \\ \frac{b_s + b_l}{2}, & T_m - \Delta T \le T \le T_m + \Delta T \\ L, & T > T_m + \Delta T \end{cases}$$

Substituting these variables in governing equation yields,

$$\frac{\partial}{\partial} = \frac{\partial}{\partial}\left(\frac{\partial}{\partial}\right) + \frac{\partial}{\partial}\left(\frac{\partial}{\partial}\right) + \frac{\partial}{\partial}\left(\frac{\partial}{\partial}\right) - \frac{\partial}{\partial}$$

The temperature-transforming model eliminates the time-step and grid-size limitations and is insensitive to the phase-change temperature range. Therefore, the model can properly handle phase change occurring over a temperature range or at a single temperature.

III. GRID GENERATION AND GRID INDEPENDENCY

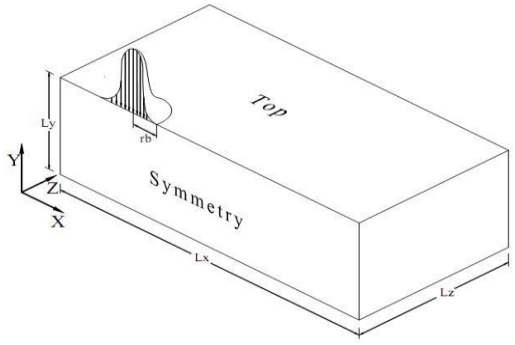

Figure 3.1: Physical model for Laser welding

In this numerical modeling of laser welding finite volume method for discretization of governing equations is used. For numerical modeling of the phase change process enthalpy method is used where the enthalpy at grid points is calculated and from these enthalpy values temperatures at corresponding points are calculated. To track solid liquid interface volume of fluid method is used where volume fraction of the cells is calculated from corresponding enthalpy values. To reduce computational time and memory, half part of welding domain is considered. 2D Welding is carried out on a mild steel sheet of size 7.5 mm X 5 mm.

The 2D model is simulated in ANSYS FLUENT. The heat source as laser beam is applied by defining a UDF and hooking it to the top boundary. To model phase change in FLUENT solidification and melting model with mushy zone constant of value 10^5 is used. The SST k-ω turbulence model is used to consider the effect of turbulence on weld pool. The pressure velocity coupling

is solved by SIMPLE algorithm with the convective terms of momentum, energy, turbulent kinetic energy and specific dissipation rate discretized using second order upwind scheme.

3.1 Assumptions

1. Gaussian heat source is considered at top surface.
2. Convection losses are considered from all surfaces except at top surface where radiations losses are also considered.
3. Material with constant thermal properties is considered.
4. Molten material is assumed to be Newtonian and incompressible.
5. The vaporization of weld metal is not considered in this case.

3.2 Governing equations

The numerical solution of heat transfer, fluid flow and other related processes can begin with the mathematical forms in which the physical laws governing these processes have been expressed.

The mathematical forms of the transport processes are often expressed as differential equations, which define certain conservation principles. Each equation employs a certain physical quantity as its dependent variable and implies that there must be a balance among the various factors that influence the variable. Examples of the physical quantity is mass, velocity and enthalpy. The general differential equation is given as,

Mass conservation equation:

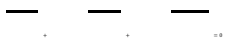

Energy equation:

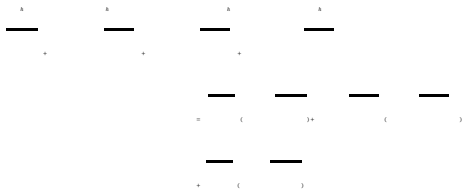

Where, $h = \int Cp*T + fl.*L$

X- Momentum equation

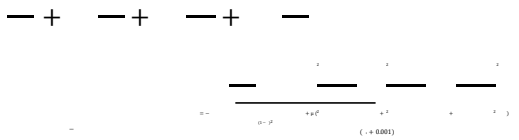

Y- Momentum equation

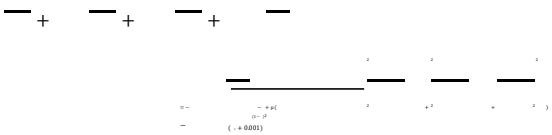

Z-Momentum equation

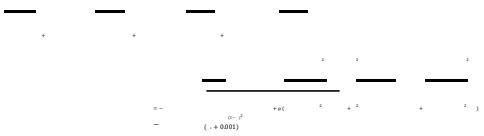

The last terms in the momentum equation correspond to enthalpy-porosity term. This is used to suppress the velocities in the solid region which act as a sink term. The variable K_o in equation is the porosity source term having a large value around 10^5. As the nodal liquid fraction approaches zero, this term becomes large and forces velocity calculation to zero as required by static solid phase.

In the Enthalpy porosity technique, there is no need to track the boundary and apply boundary conditions on the interface, as a liquid fraction whose value lies between 0 and 1 is defined depending on the enthalpy. The liquid fraction is assumed to vary linearly with enthalpy.

Where,

With these values of liquid fraction and enthalpies the temperature is calculated as,

$$\frac{h}{} , \qquad h \le h$$

$$\frac{}{} \qquad < h < h$$

$$+ \frac{h - h}{} , \qquad h \ge h$$

3.3 Boundary conditions

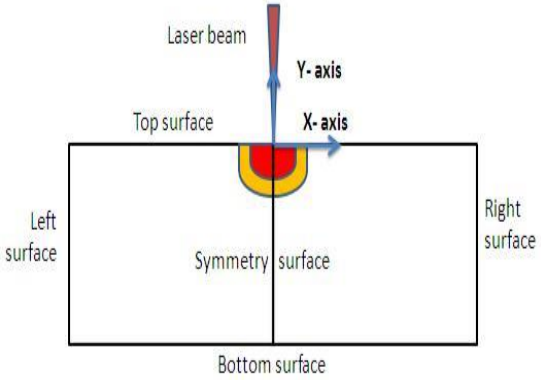

Figure 3.2: Boundary surfaces on weld plate

Because of the axis-symmetric nature of welding, the governing equations can be solved considering only half width of the work piece along weld centerline. This saves the computational memory and time required for solution.

3.3.1 Top surface

Weld top surface assumed to be flat and convection and radiation losses are assumed from top surface. The velocity boundary condition at the top is applied by equating surface tension force to viscous force at top surface as,

$$\mu \frac{}{} = \frac{} {} \frac{}{}$$

Here *u* and *v* are the velocity components along *x* and *y* directions respectively. $\partial\gamma/\partial T$ is temperature coefficient of surface tension. The *v* velocity is zero as there is no flow of liquid metal perpendicular to pool top surface. The energy balance at the top surface is,

$$= - (^4 - ^4) - h (-)$$

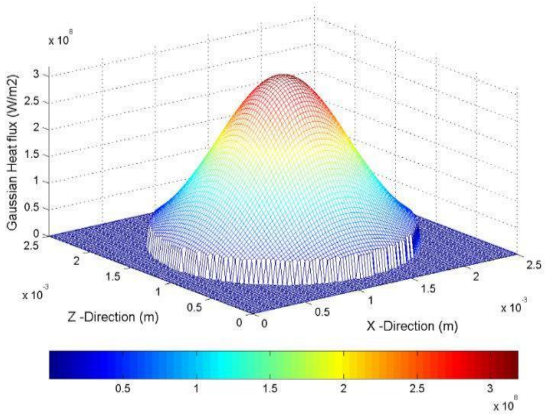

Figure 3.3: Gaussian heat flux

Gaussian laser beam as shown in figure 3.3 is given as,

$$= \frac{}{} \frac{}{} ^2 (-$$

Where *Q* is laser power, η is absorption coefficient, r_b is beam radius, *r* is the radial distance of any point on top surface from the weld source center line, σ is Stefan-Boltzmann constant, h_c is heat transfer coefficient, *Ta* is ambient temperature and *f* is heat distribution factor. The absorption coefficient has been related to electrical resistivity and wavelength of the laser radiation by following relation,

$$( ) = 0.365 (\frac{}{} ^{0.5} \frac{}{} ^{3/2} \frac{}{})$$

Where λ is the wavelength and α is the electrical resistivity of material.

3.3.2 Symmetric surface

The boundary conditions are defined with zero flux across the symmetric surface as,

$$\frac{}{} = 0, \qquad \frac{}{} = 0, = 0$$

3.3.3 Right surface

The velocities are set to be zero giving no slip boundary condition and only convective losses are considered from other surfaces.

$$= h (-)$$

3.3.4Bottom surface

The velocities are set to be zero giving no slip boundary condition and only convective losses are considered from other surfaces.

$= h (- \quad)$

$= 0, \quad = 0$

3.4 Time step for solution

For transient solution, two types of time stepping method are used namely implicit method and explicit method. In implicit method, there is only one knows value from previous time step and rest unknown values in discretized equation are obtained by solving the equations with unknown. In explicit method, there is only one unknown variable in discretized governing equation as values of the rest variable are taken from previous time step which forms a linear algebraic equation. There is limit for time step in explicit method for stability of the solution where as there is no restriction in implicit method. As implicit method is more stable in transient problems, first order transient method in FLUENT used for time step.

To solve governing equation by implicit, approach a time step has to be defined which helps in better convergence of solution. In the present investigation an fixed time stepping method is used to calculate time step depending on velocity in domain. A time step Δt_{cond} sec is used, after the melting starts the time must be reduced enough to converge the solution given by CFL condition as ,

$$\frac{}{} + \frac{}{} \leq$$

$$\leq \frac{0.5}{\frac{}{} + \frac{}{}}$$

$$\Delta t \leq \frac{1}{2\left[\frac{k}{\rho c_p}\left(\frac{1}{(\Delta x)^2} + \frac{1}{(\Delta y)^2}\right)\right]}$$

$$\Delta t = \min(\Delta t_{cond}, \Delta t_{melt})$$

Where C_{max} is courant number which less than or equal to 1 for explicit scheme. In this case depending on the grid size and maximum velocities observed from literature a fixed time step of 0.0005 sec is used.

The mesh is generated in ICEM CFD software using blocking method to generate quad elements. The complete domain is divided in number of quad type cell elements. To have better convergence and resolution of weld pool shape a fine mesh is required, but this will increase the number of cell in the domain and the computational time for the simulation. Therefore, a grid independency test is carried out where, mesh with decreasing grid size is simulated and the results obtained from each case are compared. Here four grid sizes are compared as shown in the table 3.1.

Table 3.1: Mesh details

Minimum grid size	Cell count	Mesh Quality	
		Orthogonal quality	Aspect ratio
0.1 mm	2856	1.0	2.014
0.075mm	5934	1.0	1.6784
0.05 mm	11514	1.0	1.9526

As laser welding shows a localized heat zone near the laser beam application area, the mesh need to be refined at the center. Figure 3.4 shows fine mesh at the center and slightly coarse mesh on the left and right side of domain as these zones don't show much change in temperature.

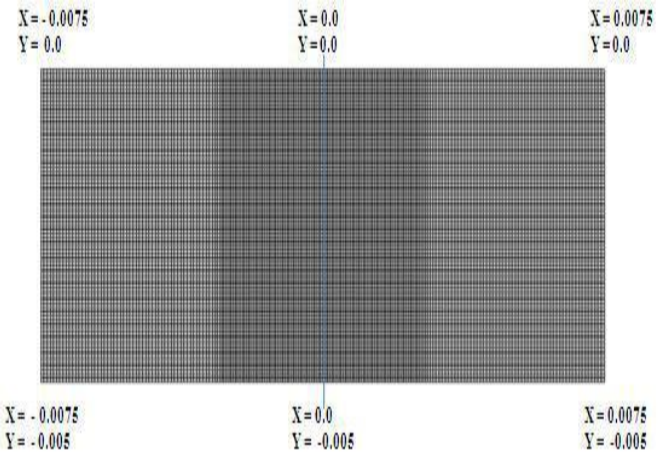

Figure 3.4: Structured mesh of plate

In this analysis only the left half portion is considered and the other portion is solved using symmetry condition. The velocity and temperature at distance of y = 0.0002 m, y = 0.0004 m y= 0.006 m, y = 0.008 m and y = 0.001 m from the top surface are compared as below:

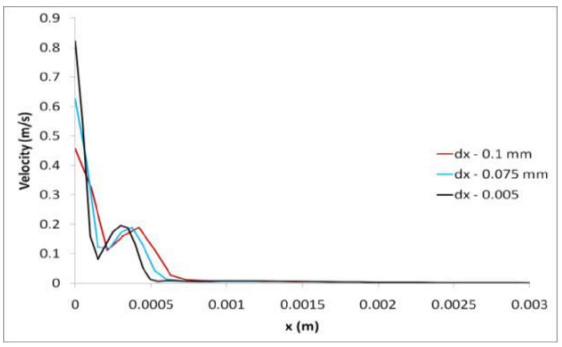
Velocity (m/s)
x (m)
dx - 0.1 mm
dx - 0.075 mm
dx - 0.005

(a)

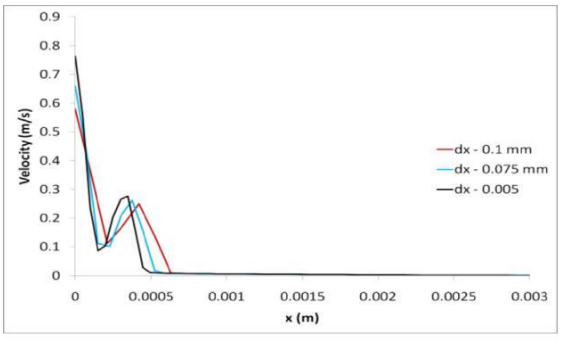
Velocity (m/s)
x (m)
dx - 0.1 mm
dx - 0.075 mm
dx - 0.005

(b)

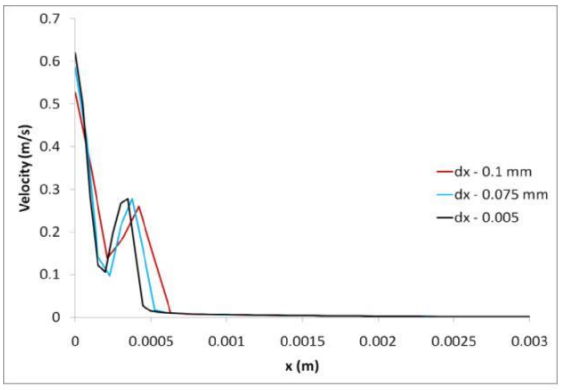
Velocity (m/s)
x (m)
dx - 0.1 mm
dx - 0.075 mm
dx - 0.005

(c)

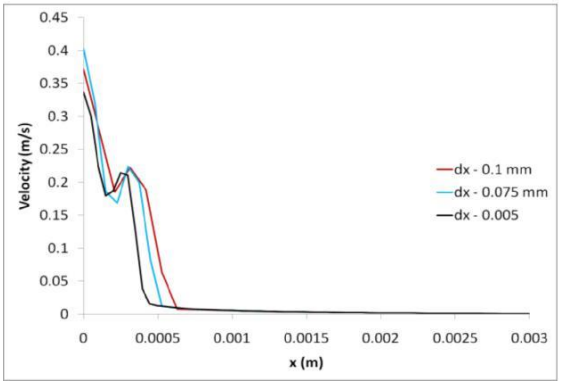
Velocity (m/s)
x (m)
dx - 0.1 mm
dx - 0.075 mm
dx - 0.005

(d)

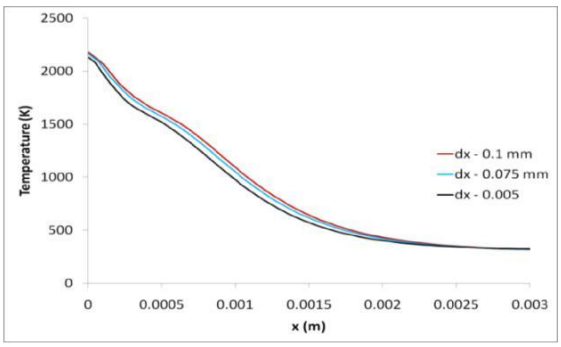
Temperature (K)
x (m)
dx - 0.1 mm
dx - 0.075 mm
dx - 0.005

(e)

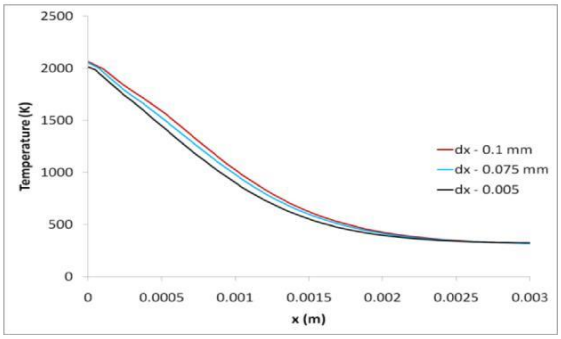
Temperature (K)
x (m)
dx - 0.1 mm
dx - 0.075 mm
dx - 0.005

(f)

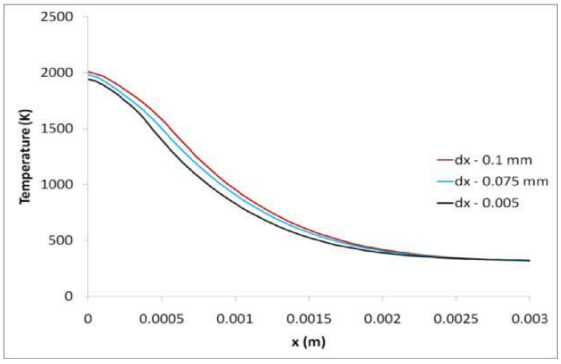
Temperature (K)
x (m)
dx - 0.1 mm
dx - 0.075 mm
dx - 0.005

(g)

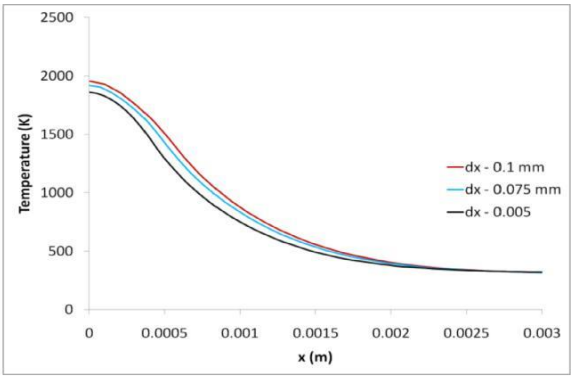
Temperature (K)
x (m)
dx - 0.1 mm
dx - 0.075 mm
dx - 0.005

(h)

Figure 3.5: Grid Independency results. Figure a, b, c, d shows velocity plots at y = 0.0002, y = 0.0004, y = 0.0006 and y = 0.0008 m respectively from top surface. Figure e, f, g, h shows temperature plots at y = 0.0002, y = 0.0004, y = 0.0006 and y = 0.0008 m respectively from top surface.

As observed in the figure 3.5 the velocity magnitude and temperature plots at different grid size show change in values because of fine mesh. The temperature shows peak values at the center point of the laser beam and decreases gradually also, the difference in temperature with grid size is less with finer mesh. The velocity plots show sharp change in values with finer grid size. The results with minimum grid size 0.025 mm shows better of velocity and temperature than other grid sizes therefore, the mesh with grid size of 0.025 mm was selected for further analysis.

Table 3.2: Thermo-physical properties of mild steel

Property	Value	Units
Density	7400	kg/m^3
Conductivity	59	W/m-K
Specific heat	586	J/kg-K
Dynamic viscosity	0.00578	Pa-s
Latent heat	272000	J/kg
Surface tension coefficient	0.0005	N/m-K
Solidus temperature	1523	K
Liquids temperature	1723	K
Heat transfer coefficient	10	W/m^2K

IV. RESULTS AND DISCUSSIONS

For observing the effect of laser beam parameters, beam power and beam radius on the weld pool shape, analysis is carried out for laser spot welding process with spot time of 0.1 sec. The evolution of weld pool with time is also studied for beam power of 2000 W and beam radius of 0.001 m. The cases considered for analysis are as follows:

Table 4.1 Cases for analysis

Case	Laser beam power (W)	Laser beam radius (m)
Case – 1	1000	0.001
Case – 2	1000	0.000875
Case – 3	1000	0.00075
Case – 4	1000	0.000625
Case – 5	1000	0.0005
Case – 6	1250	0.001
Case – 7	1250	0.000875
Case – 8	1250	0.00075
Case – 9	1250	0.000625
Case – 10	1250	0.0005
Case – 11	1500	0.001
Case – 12	1500	0.000875
Case – 13	1500	0.00075
Case – 14	1500	0.000625
Case – 15	1500	0.0005
Case – 16	1750	0.001
Case – 17	1750	0.000875
Case – 18	1750	0.00075
Case – 19	1750	0.000625
Case – 20	1750	0.0005
Case – 21	2000	0.001
Case – 22	2000	0.000875
Case – 23	2000	0.00075
Case -24	2000	0.000625
Case -25	2000	0.0005

4.1. Temporal evolution of weld pool

To study the transient behavior of weld pool, shape a case is considered with laser beam power of 2000 W and beam radius of 0.001 m. This can be studied by observing the volume of fraction (VOF) contours of the domain.

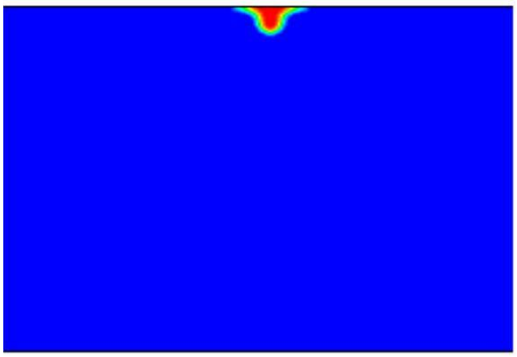

(a)

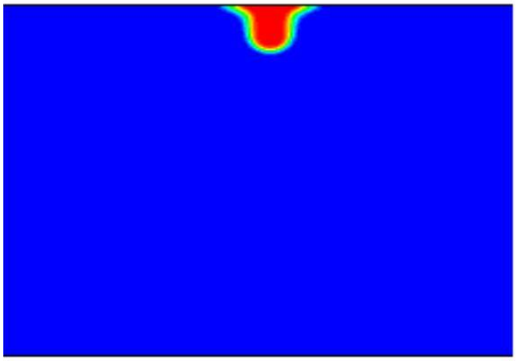

(b)

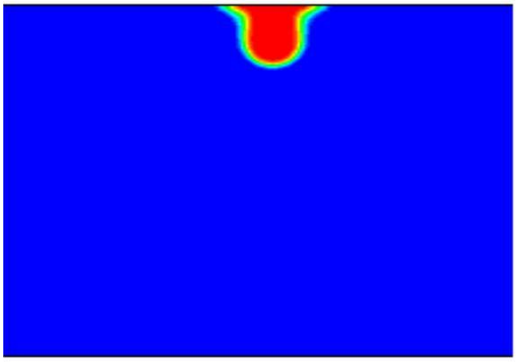

(c)

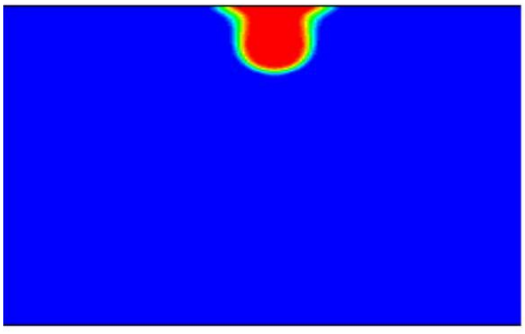

(d)

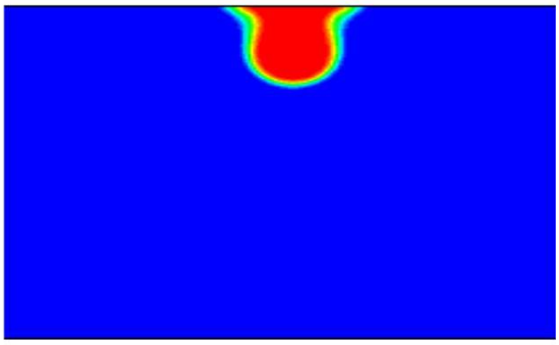

(e)

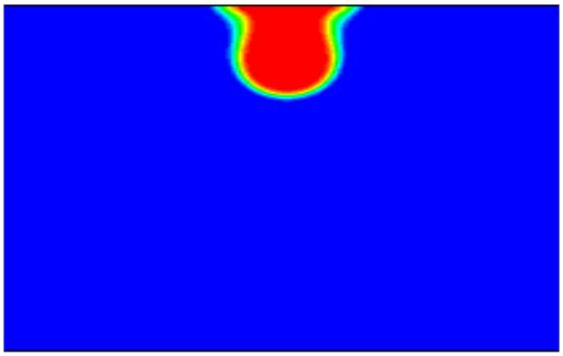

(f)

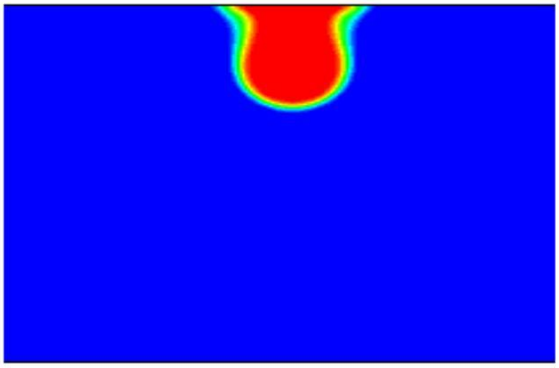

(g)

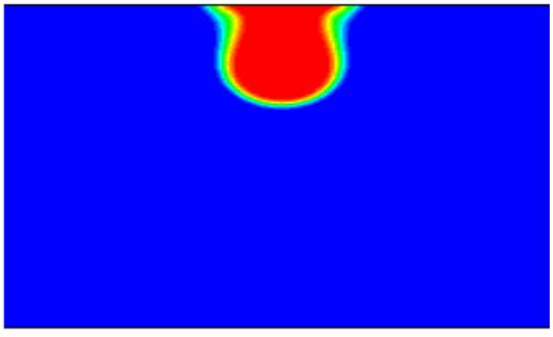

(h)

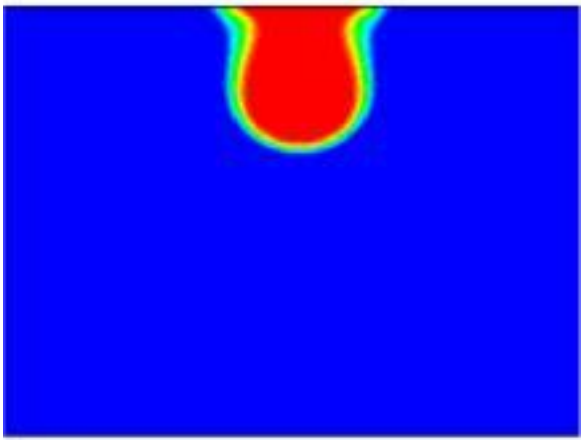

(i)

Figure4.1: Contours of volume fraction at (a) 0.02s, (b) 0.03s, (c) 0.04s, (d) 0.05s, (e) 0.06s, (f) 0.07s, (g) 0.08s, (h) 0.09s, (i) 0.1s.

The Fig. 4.1 shows change in the weld pool shape with time. As the heat is applied on the top surface by the laser beam its temperature starts increasing, as the temperature increases above the solidification temperature the material starts melting. This localized melting at the top surface leads to the fluid flow which is Marangoni effect created to the large temperature gradient at the top surface as shown in figure 4.2.

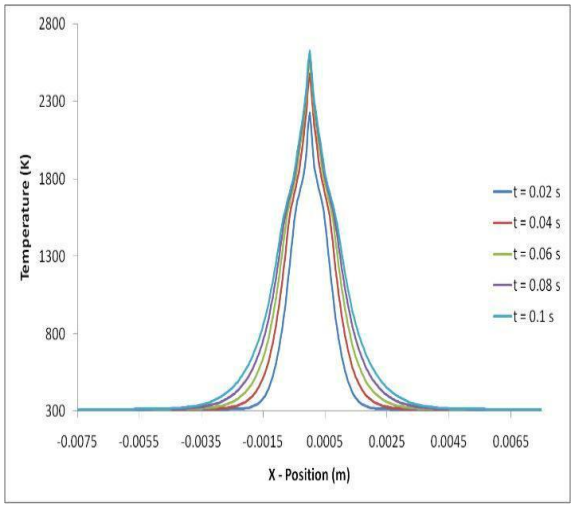

Figure 4.2: Temperature profile at top surface for case 21

Initially a conical shape of pool is seen due to localized heating effect by the laser beam. The conical shape is formed due to the Gaussian distribution of heat flux at the top surface with the peak temperature at the center of the beam, as the time progresses the conical shape is deformed to a tubular shape.

This tubular shape is the effect of the velocity vectors directing the melt pool at the top surface to the center of the pool and from the top center, the melt fluid is directed towards the bottom of the weld pool carrying the heat from the top to the bottom of the pool, heating the bottom portion and again flowing in the upward direction. The flow pattern creates vortices along the center line of the weld pool. The tubular shape grows with time as more heat is carried to the bottom of the weld pool. The tubular shape then starts deforming and a bulge is observed in the bottom portion with a neck region separating the bottom bulge from the top conical part.

The bulge is due to the resistance offered to the melt pool by the solid region of the material as the fluid flowing in the upward direction carries less heat to melt the region and thus forming a neck at the top. The flow direction can be seen by velocity vector plot from fig 4.3

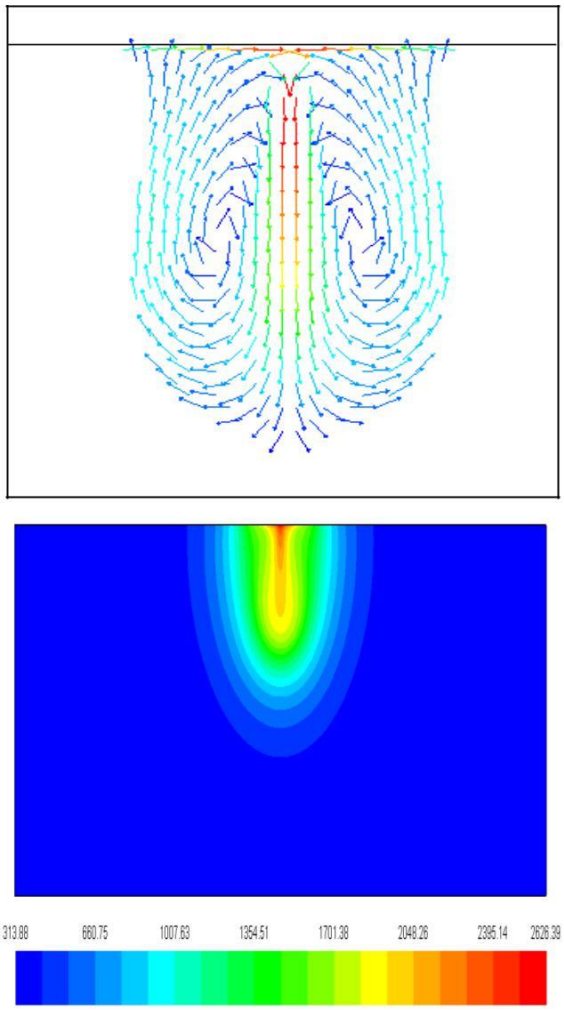

Figure 4.3: Velocity vector and temperature contour in the weld pool at t = 0.01 s

4.2. Effect of beam power and beam radius on weld pool depth

Weld depth is an important parameter in welding study as the depth of weld decides its strength. Therefore the effect of beam power on weld depth is studied by varying the beam power from 1000 W to 2000 W.

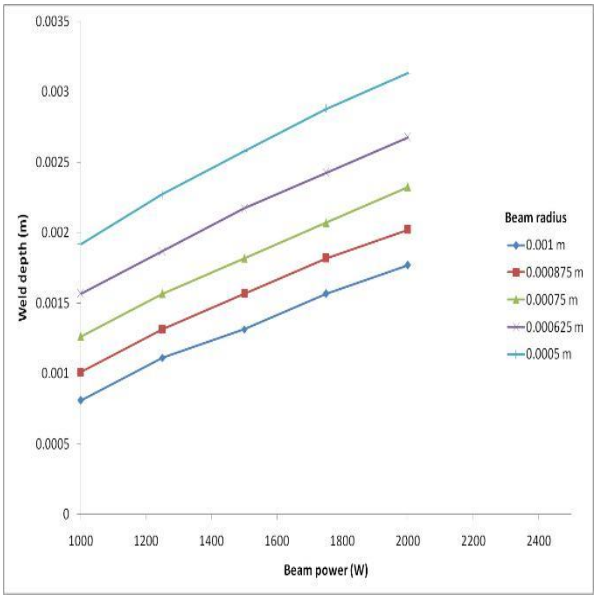

Graph 4.1: Effect of beam power and beam radius on weld depth

Graph 4.1 shows that with increase in beam power the weld depth increases as more energy is applied to the material. The increase in weld depth with power is liner which shows its direct dependence. Also with the decrease in beam radius the weld depth increases, this is due to the Gaussian nature of the heat source where the beam distribution is exponential with the beam radius in the exponential part of the equation.

Therefore, with decrease in beam radius the temperature distribution becomes steeper and the temperature gradient at the top increases with decreasing beam radius. As the velocity vectors of melt pool at top depend on this temperature gradient, more momentum is added to the weld pool leading to an increase in weld depth.

The vaporization temperature of mild steel is around 3000 K therefore, monitoring maximum temperature is essential as vaporization may form air pockets in weld during solidification.

Table 4.2: Tabulated results

Case	Input parameter		Output parameter		
	Beam power (W)	Beam radius (m)	Maximum Temperature (K)	Maximum velocity (m/s)	Weld depth (m)
Case-1	1000	0.001000	1905.7201	0.51813486	0.00080808
Case-2	1000	0.000875	2040.9489	0.63341736	0.00101010
Case-3	1000	0.000750	2212.3824	0.75602669	0.00126263
Case-4	1000	0.000625	2444.9433	0.89016472	0.00156566
Case-5	1000	0.000500	2772.6908	1.0506372	0.00191919
Case-6	1250	0.001000	2068.1962	0.65398415	0.00111111
Case-7	1250	0.000875	2226.2126	0.75997865	0.00131313
Case-8	1250	0.000750	2414.1243	0.87434509	0.00156566
Case-9	1250	0.000625	2672.1909	1.0048051	0.00186869
Case-10	1250	0.000500	3033.5119	1.1646373	0.00227273
Case-11	1500	0.001000	2215.8275	0.75200284	0.00131313
Case-12	1500	0.000875	2388.1522	0.85489064	0.00156566
Case-13	1500	0.000750	2592.959	0.96517204	0.00181818
Case-14	1500	0.000625	2871.8109	1.0961106	0.00217172
Case-15	1500	0.000500	3270.4286	1.2590066	0.00257576
Case-16	1750	0.001000	2358.6626	0.83395558	0.00156566
Case-17	1750	0.000875	2529.9121	0.9295781	0.00181818
Case-18	1750	0.000750	2755.0694	1.0415489	0.00207071
Case-19	1750	0.000625	3057.0346	1.1746185	0.00242424
Case-20	1750	0.000500	3491.1148	1.3411307	0.00287879
Case-21	2000	0.001000	2476.7543	0.89898666	0.00176768
Case-22	2000	0.000875	2669.0501	0.99636795	0.00202020

Case-23	2000	0.000750	2907.8456	1.1089582	0.00232323
Case-24	2000	0.000625	3229.6932	1.2440949	0.00267677
Case-25	2000	0.000500	3701.2116	1.4143615	0.00313131

Table 4.2 shows that the maximum temperature increases with increase in beam power and decrease in beam radius. The maximum temperature in case-10, case-15, case-19, case-20, case-24 and case-25 is above 3000 K. This shows the beam parameters to be considered for welding mild steel with vaporization of the weld material. In many cases the maximum velocity is above 1 m/s, which shows larger momentum gain of the weld pool and maximum distribution of heat within the weld pool.

4.3 Weld pool shape

Below figures shows weld pool shape at 0.1s for cases simulated as shown in the table

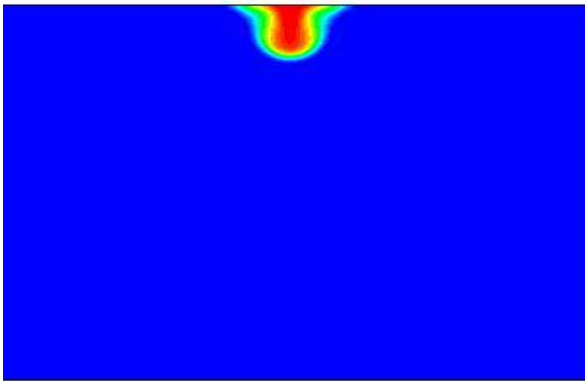

(a) Case-1

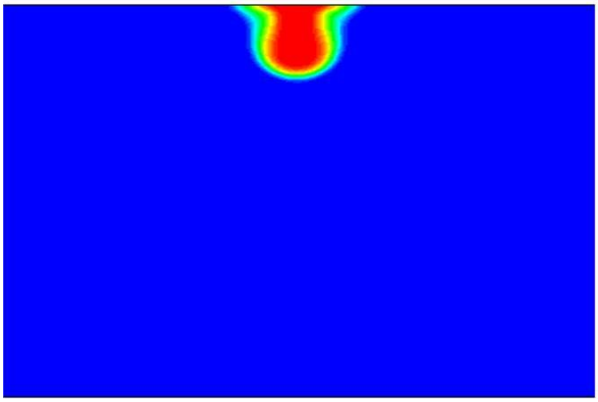

(b) Case-2

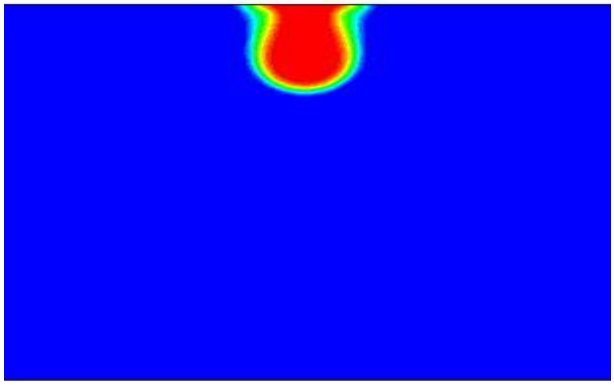

(c) Case-3

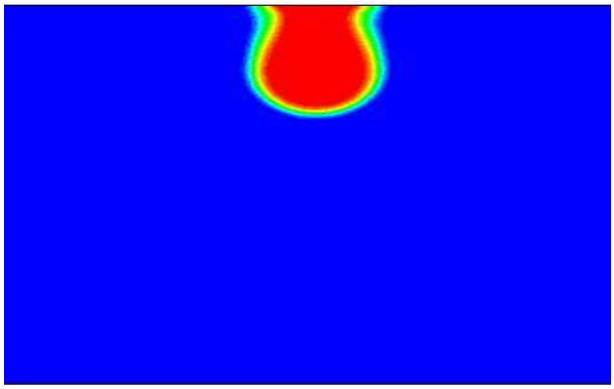

(d) Case-4

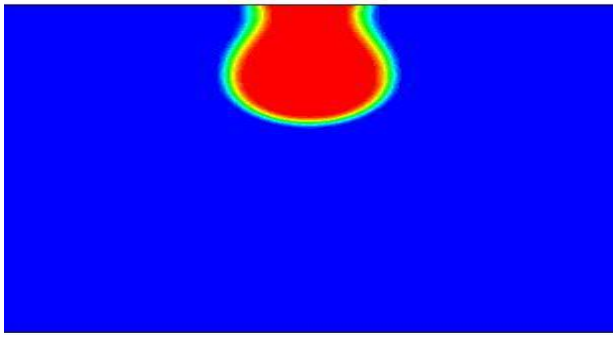

(e) Case-5

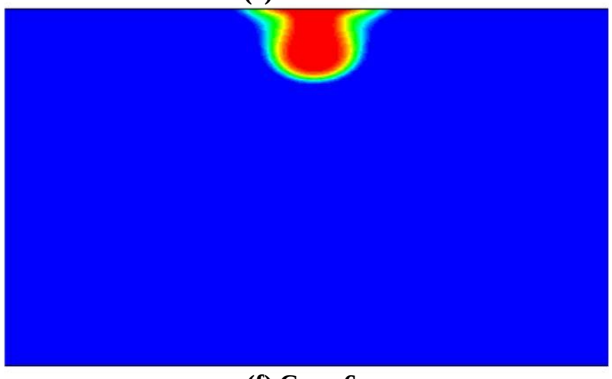

(f) Case-6

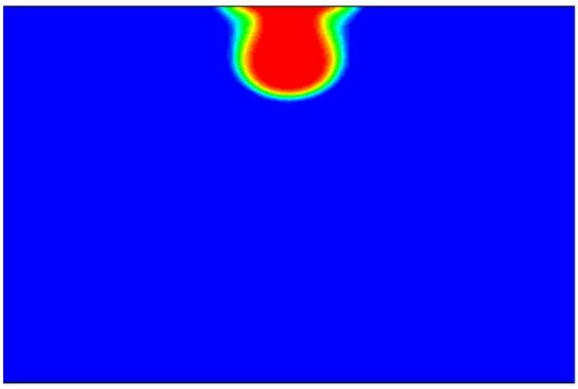

(g) Case-7

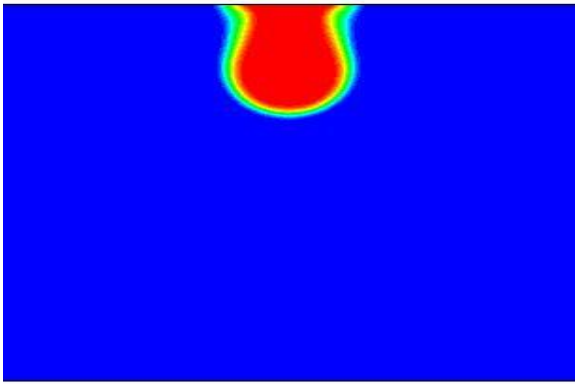

(h) Case-8

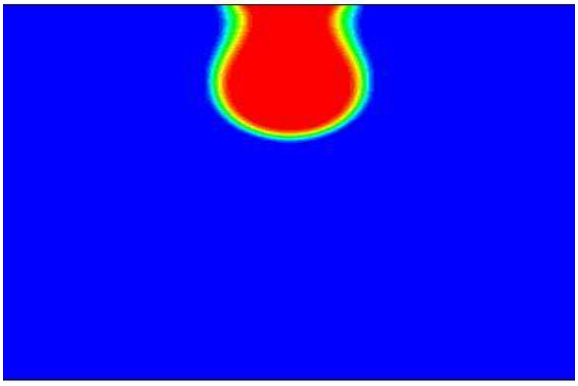

(i) Case-9

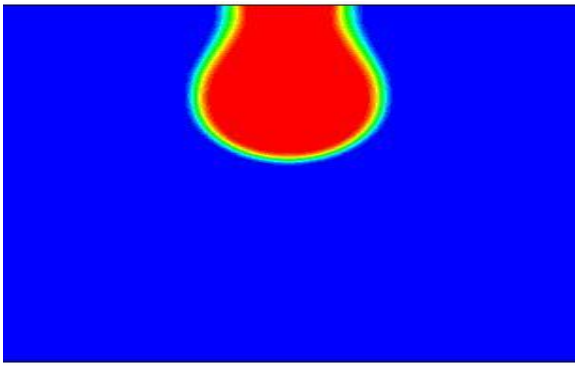

(j) Case-10

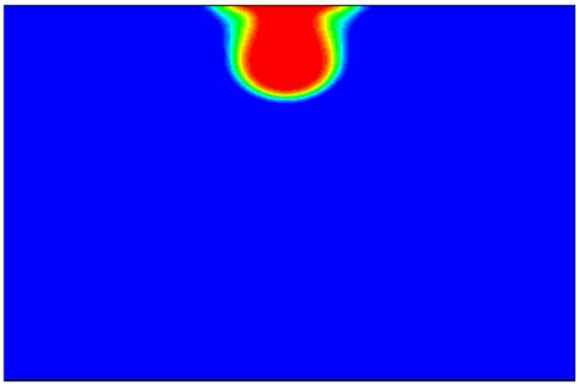

(k) Case-11

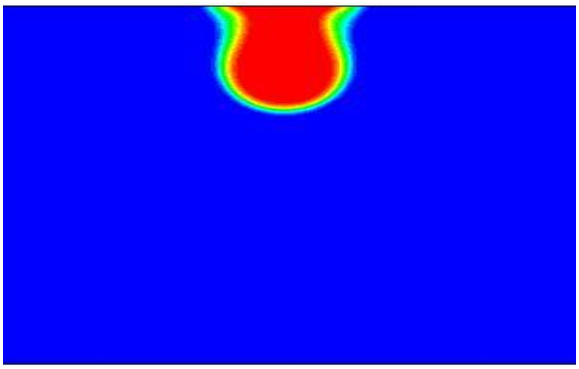

(l) Case-12

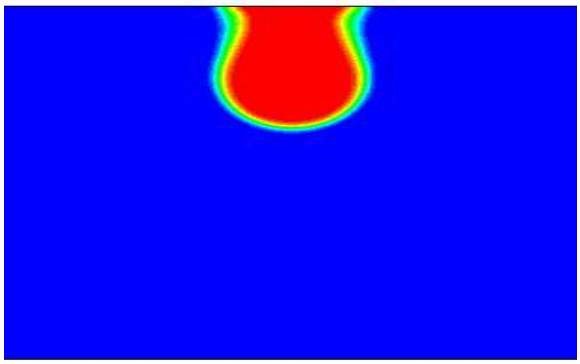

(m) Case-13

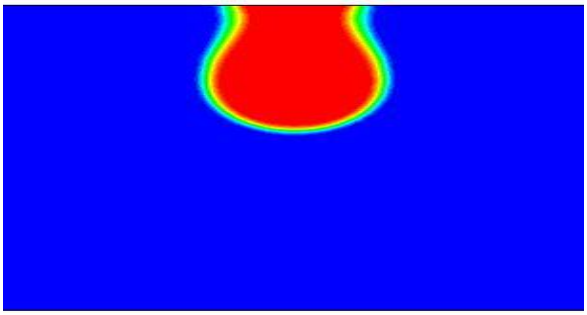

(n) Case-14

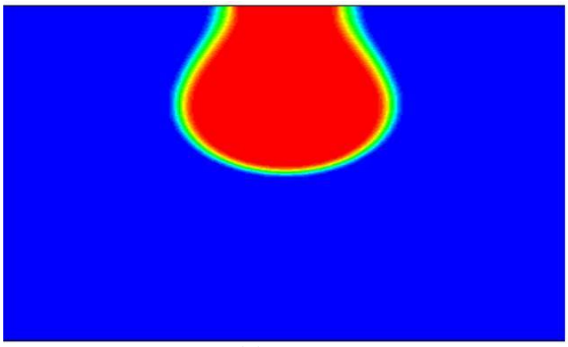

(o) Case-15

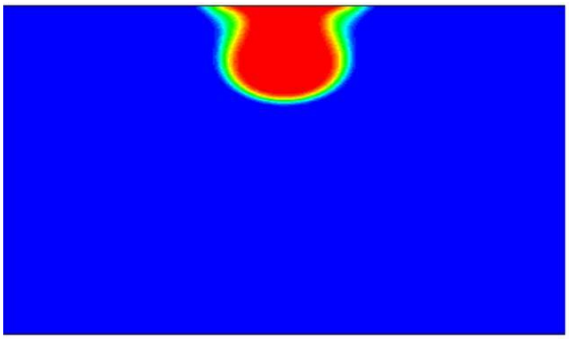

(p) Case-16

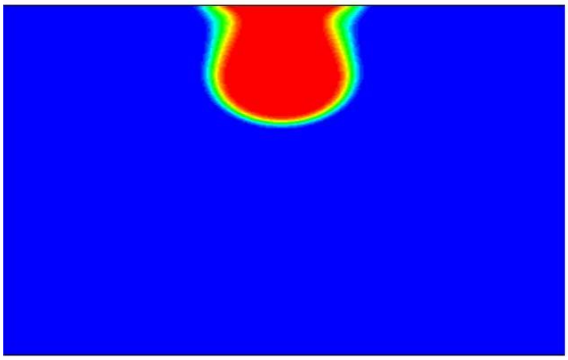

(q) Case-17

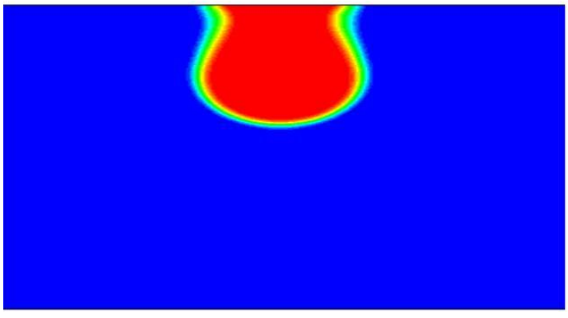

(r) Case-18

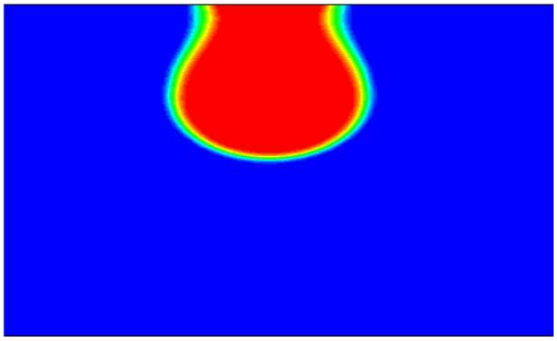

(s) Case-19

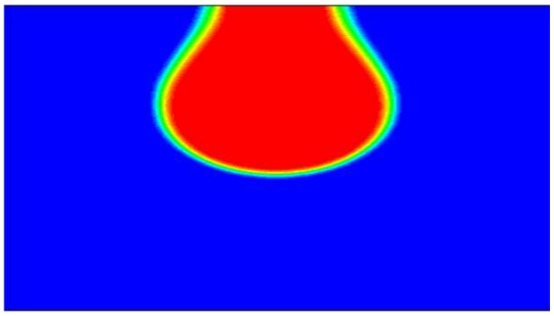

(t) Case-20

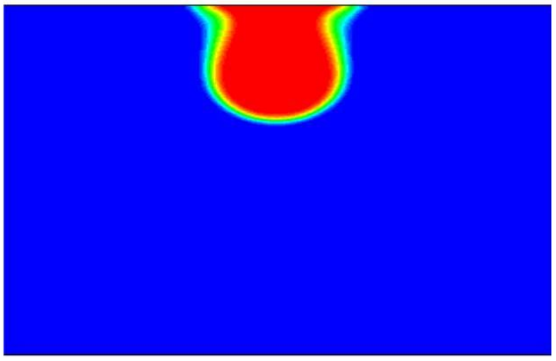

(u) Case-21

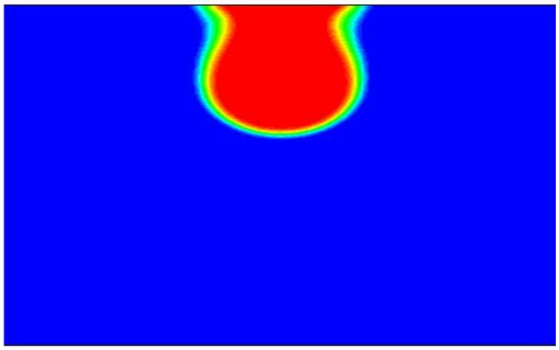

(v) Case-22

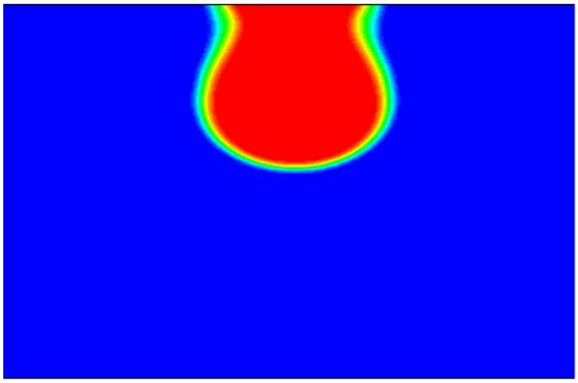

(w) Case-23

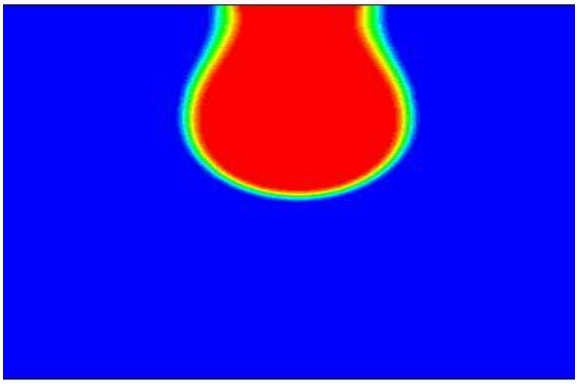

(x) Case-24

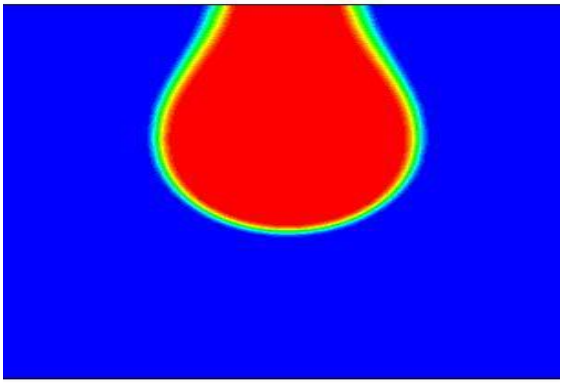

(y) Case-25

Figure 4.4: Weld pool shape

The figure 4.4 shows weld pool formed at 0.1s after the initiation of the welding. The case with low power and high beam radius show tubular shape weld pool whereas, the cases with high beam power and low beam radius show bulb shaped weld pool. This is due to more energy drawn to the bottom of the weld pool.

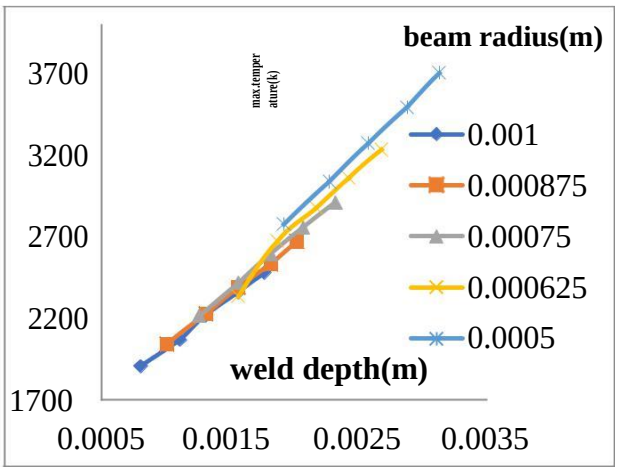

Graph 4.2 showing a linear relation between weld depth and max.temperature at different beam radius.

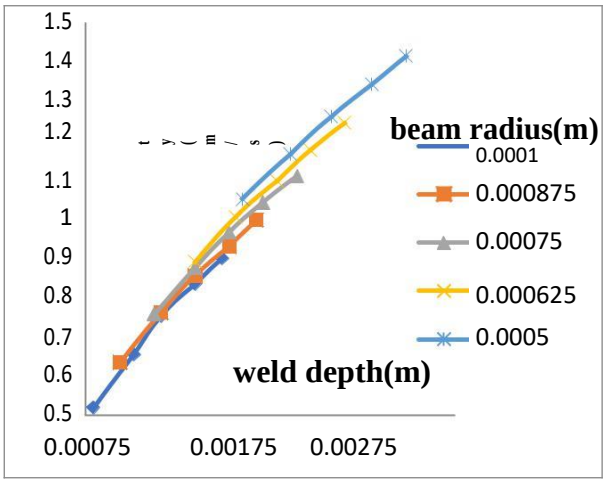

Graph 4.3 showing a linear relation between weld depth and beam velocity at different beam radius.

Graphs 4.2 and 4.3 shows that with increase in beam power from 1000W to 2000W and by decrease in beam radius from 0.001m to 0.0005m there is an increase in weld depth and maximum temperature induced which is a linear relation. Similarly, the velocity of the weld pool also increases which is again a linear relation between weld depth and velocity this is due to the Gaussian nature of the heat source with completely concentrated beam power the temperature induced will increases.In previous studies, it is seen that heat affected zone varies with heat input. In this work, it is clearly observed in graphs.4.2 & 4.3 that with increasing power weld depth increases with increase in temperature i.e. Heat input. Keeping these two-contradicting statements in mind the

optimum temperature is 2871 K (case-14) with laser beam radius 0.000625 m (power 1500 w). Though the highest temperature is observed only on laser beam radius 0.0005 m (power 2000 w) but heat affected zone also increases here as the heat input is the highest.

V.CONCLUSIONS

1. From the results it is seen that laser beam power affects the shape of weld pool as increasing beam power increases the pool depth.
2. The beam radius also affects the shape of the weld pool as with the decrease in beam radius, weld depth increased and so increases pool width.
3. The maximum temperature increases with increase in beam power and decrease in beam radius.
4. The maximum velocity increases with increase in beam power and decrease in beam radius.
5. The weld pool shape changes with time from conical to tubular and finally to bulb shape pattern for higher beam power and lower beam radius.
6. The temperature distribution is highly localized showing temperature rise only in the region near laser beam application area.

REFERANCES

1) **J. MAZUMDER, W. M. STEEN**, 1979, 'Heat transfer model for CW laser material processing'*Journal of Applied physics*, vol. **51**, 941-947.
2) **C. PRAKASH, M. SAMONDS, A. K. SINGHAL**, 1987, 'A fixed grid numerical methodology for phase change problems involving a moving heat source', *International journal of heat and mass transfer*, vol. **30**, 2690-2694.
3) **G. A. TAYLOR, M. HUGHES, N. STRUSEVICH, K. PERICLEOUS,** 1999, 'Finite volume methods applied to the computational modeling of welding phenomenon,' *Second international conference on CFD in minerals and process industries*, 405-410.
4) **T. F. CHENG**, 1999, 'A numerical simulation for two-dimensional moving boundary problems with a mushy zone', *Computational mechanics*, vol. **23**, 440-447.
5) **W. S. CHANG**, S. J. NA, 2002, 'Numerical and experimental investigation of laser beam welding', *Metallurgical and materials transactions*, vol. **33B**, 757-764.
6) **R. BROCKMANN, K. DICKMANN, P. GESHAV& K. MATTHES**, 2003, 'Calculation of temperature field in a thin moving sheet heated with laser beam', *Optics and laser technology*, vol. **35**, 115-122.
7) **J. F. LI, L. LI, F. H. STOTT**, 2004, 'A three-dimensional numerical model for a convection diffusion phase change process during laser melting of ceramic materials', *International journal of heat and mass transfer*, vol.**47**, 5523-5539.
8) **J. C. ION**, 2005, '*laser processing of engineering materials*', 263.
9) **X. HE, J. W. ELMERAND T. DEBROY**, 2005, 'Heat transfer and fluid flow in laser micro-welding', *Journal of applied physics*, vol. **97**, 1-9.
10) **HAN GUO MING, ZHAO JIAN, LI ZIANQANG**, 2007, 'Dynamic simulation of the temperature field of stainless steel laser welding', *Materials and design*, vol. **28**, 240-245.
11) M.SUNDAR,A.K.NATH,D.K. BANDYOPADHYAY, S. P. CHOUDHARY, P. K. DEYAND D. MISHRA, 2007, 'Numerical simulation of melting and solidification in laser welding of mild steel', *International journal of computational materials science and surface engineering*, vol. **1**, 717-733.
12) **YI-CHUN LIAO, MING-HUEI YU**, 2007, 'Effects of laser beam energy and incident angle on the pulse laser welding of stainless steel thin sheet', *Journal of materials processing technology*, vol. **190**.
13) **OKAMOTO, GILLNER, OLOWINSKY, GEDICKEAND UNO**, 2008, 'Fine micro-welding of thin stainless-steel sheet by high speed laser scanning', *Journal of Laser Micro/Nan engineering*, vol. **3**, 95-99.
14) **S. Z. SHUJA, B. S. YILBAS, O. MOMIN**, 2011, 'Laser heating of a moving slab: Influence of laser intensity parameter and scanning speed on temperature field and melt size', *Optics and lasers in engineering*, vol. **49**, 265-272.
15) **Pawan Kumar,Kishor P Kolhe, Sham H Mankar, Sanjay Kumar,** 2015 'Prediction of Heat affected zone and effect of heat input in GTA Welded Al Alloy 6061, '*International Journal of Engineering Science and Innovative Technology' Volume4, Issue6.*